Available online at www.sciencedirect.com
SCIENCE DIRECT
International Journal of Multiphase Flow 32 (2006) 499–516
International Journal of Multiphase Flow
www.elsevier.com/locate/ijmulflow

Application of a borescope to studies of gas–liquid flow in downward inclined pipes

E. Roitberg (Trostinetsky), L. Shemer, D. Barnea *

Department of Fluid Mechanics and Heat Transfer, Faculty of Engineering, Tel-Aviv University, Tel-Aviv 69978, Israel

Received 15 April 2005; received in revised form 19 January 2006

Abstract

The aim of the present study is to investigate stratified downward gas–liquid pipe flow with a non-intrusive measurement technique that is based on a borescope connected to a digital video camera. The borescope-based technique enables to determine the instantaneous cross-sectional distribution of both phases within the pipe. Water and air were used as working fluids. Quantitative data was extracted from sequences of recorded video images by applying a developed data processing technique for instantaneous gas–liquid interface boundaries determination. Experiments were performed for a wide range of downward pipe inclinations and gas and liquid flow rates. The instantaneous and time-average cross-sectional holdup for each set of flow parameters was calculated. Particular attention was given to the study of the interface shape that in many occasions was not flat and was characterized by the penetration of the liquid along the pipe periphery. Temporal variation of the surface elevation was also studied and various regimes characterizing interfacial waves were defined using both the recorded time series of the instantaneous depth of the water layer and the Fourier analysis of those records.

Keywords: Two-phase pipe flow; Downstream stratified flow; Borescope image processing; Cross-sectional interfacial shape

1. Introduction

Two-phase (gas–liquid) flow in horizontal or downward inclined pipes is often stratified with the liquid occupying the bottom part of the pipe. This flow regime is usually observed when gas and liquid flow rates are sufficiently low. One of the most intriguing problems in two-phase stratified flow is the distribution of the liquid film around the circumference in horizontal and inclined pipes. Transition from stratified smooth to stratified wavy, as well as the transition from stratified to non-stratified slug or annular flow depends strongly on the film thickness and on the film shape. Experimental measurements of these parameters, especially near the transition zone, are quite rare. Calculations of the film thickness distribution in the pipe cross-section are usually complicated and require application of phenomenological models. For horizontal and

* Corresponding author. Tel.: +972 3 640 8504; fax: +972 3 640 7334.
E-mail address: dbarnea@eng.tau.ac.il (D. Barnea).

0301-9322/$ - see front matter © 2006 Elsevier Ltd. All rights reserved.
doi:10.1016/j.ijmultiphaseflow.2006.01.005

downward slightly inclined flow, stratified – slug transition takes place at relatively high liquid flow rates, whereas stratified – annular transition occurs at high gas flow rates. At steep downward inclinations, stratified – annular transition is observed even at very low gas flow rates. The knowledge of the gradual variation of the instantaneous and average film thickness and of the interfacial shape, up to the transition to annular or slug flow, is of utmost importance for understanding the mechanism of the flow pattern transition. In addition, the knowledge of the film shape for various operational conditions is required for pressure drop, as well as for heat and mass transfer calculations.

Barnea et al. (1982) conducted experiments in two phase flow in downward inclined pipes. They found that stratified smooth flow is not observed when the downward pipe inclination angle exceeds about 5°. They also noticed that for downward flow, (contrary to horizontal or slightly-inclined upward pipe flow, where waves are generated due to the wind action over the interface) natural instability occurs for almost pure gravity-driven downward flow without or with negligible gas flow rates. The inception of those waves and their properties depend on the liquid flow rate and the level and shape of the interface that is strongly dependent on pipe inclination. Barnea et al. (1982) used the critical Froude number as a criterion for transition from smooth to wavy stratified flow in the region of low gas flow rates. Analysis of Giovine et al. (1991) indicates that a certain threshold value of the liquid depth should be attained for the interface to become unstable in downward liquid flow. In downward pipes at steep inclinations, Barnea et al. (1982) speculated that the mechanism by which stratified flow is transferred to annular flow at low gas flow rates is due to liquid droplets torn away from the wavy turbulent interface and thrown upon unwetted tube walls, eventually leading to annular flow.

The available experimental data on the liquid–gas interfacial shape in separated flows as a function of pipe diameter, pipe inclination and flow rates of both phases is rather limited. Luninski et al. (1983) used a number of resistance probes at the circumference of the pipe to study film thickness distribution along the pipe cross-section periphery in horizontal pipes of small diameter. Paras et al. (1994) measured the variation of the film thickness in the pipe cross-section at the angles $\alpha = 0°$ and $\alpha = 45°$ (relative to the vertical) by using parallel wire conductance probes. Measurements were carried out in the region of stratified atomization flow, namely at relatively high gas flow rates. Recently fiber-optic based borescopes, or endoscopes, were applied for obtaining cross-sectional data on phase distribution in two-phase flow studies. Angeli and Hewitt (2000) used a video recording technique with an endoscope in their investigation of the drop size distribution in horizontal oil–water dispersed flows. Wojtan et al. (2003) suggested the use of an endoscope for dynamic void fraction measurements in stratified flows.

The purpose of this study is to apply video recording of a sequence of borescope images to perform quantitative measurements of the instantaneous distribution of the liquid and gas phases in the pipe cross-section in downward flow.

2. Experimental set-up and procedure

Experiments are carried out in a 10 m long transparent Perspex pipe. The pipe has an internal diameter of $D = 24$ mm and consists of 2 m long sections, connected by flanges. The carefully leveled pipe is placed on a steel frame that can be fixed by a hydraulic system at any angle of inclination. The inclination angle was measured with a high precision ($\pm 0.1°$) by a digital angle level. The schematic description of the experimental facility is presented in Fig. 1.

Water and air are used as working fluids. The water and air supply systems work independently. The facility allows supplying both air and water from either end of the pipe, thus upward flow in the range of 0 to 90° as well as downward flow in the range 0° to −90° can be obtained by reversing inlet and outlet. Countercurrent two phase flow can be obtained as well. In the present study, co-current air–water flow was studied for downward inclination angles up to 50°. The entrance section is of a splitter plate type, with water flowing below and gas above the plate, thus creating stratified downward flow at the entrance. The pipe outlet is open to atmosphere.

Water is circulated through the system in a closed loop by a frequency-controlled centrifugal pump with a capacity of 10 m^3/h at 33 m total head. Water is supplied from a tank filled with tap water supplied via an ion exchanger filter. High-pressure main serves as an air source. Air passes through an oil filter and a pressure reducer, before its entrance to the pipe. The pressure reducer sustains a constant entrance gage pressure of

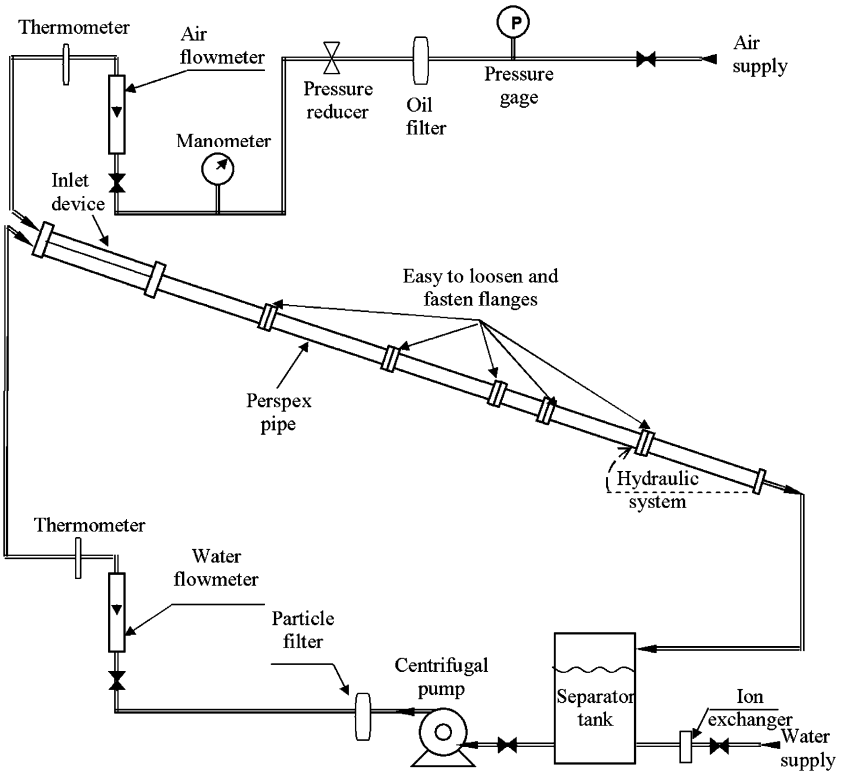

Fig. 1. Layout of the experimental facility.

1 bar. Inlet volumetric flow rates of water and air are determined by a set of rotameters. The air and water are injected at room temperature of 23 °C. The error in gas and liquid superficial velocities determined by the rotameter readings is estimated not to exceed 10%.

The measurements in the present study use a combination of a borescope, based on fiber optic technology, and a light-sheet illumination by a laser. The borescope is a non-intrusive technique that practically does not interfere with the flow. To perform continuous visualization and recording of the phase distribution in the illuminated plane, the borescope is connected to a digital video camera using a special adapter. Two cameras were used in the present experiments. In most cases, 25 fps Sony color digital video camera with resolution of 352 by 288 pixels was used. In some cases where either higher resolution or a faster speed were required, fast Pixelink black and white video camera with resolution of 1280 by 960 pixels was applied. This camera was operated at the recording rate of 50 fps. The continuous sampling duration for each working condition was about 1 min for the Sony camera and about 1.4 min for Pixelink camera.

The main advantage of the borescope for two-phase flow measurements is in its ability to visualize the distribution of both phases in the whole cross-section of the pipe. As our preliminary attempts demonstrated, the application of this instrument is however not straightforward and is subject to severe limitations. After many attempts it became clear that quantitative results can only be obtained when there is a single phase with a constant refraction index between the borescope lens and the illuminated cross-section. This limitation allows to study in detail mainly separated gas–liquid flows, such as stratified regime (smooth or wavy), or the shape of elongated bubbles in slug flow both in downward and upward flow.

The view angle of the borescope used in this study is 40°. The borescope is inserted into the upper part of the pipe flush with the pipe wall at an angle of 20° relative to the pipe axis. A special borescope support module was constructed for this purpose. Schematic description of the borescope set-up is shown in Fig. 2. The borescope focusing range extends from 2 mm to infinity and has considerable focus depth. Light sheet illumination is applied to select a well-defined imaged plane. A 4 W Argon laser is used as a light source to generate light sheet illumination of a thin cross-section of the pipe that is normal to the pipe wall. The laser and the

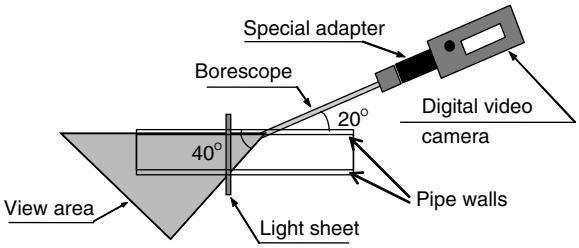

Fig. 2. Flow visualization system.

light sheet generating optics, as well as the support of the borescope and the connected to the borescope eye-cup lens video camera, are attached to the steel frame of the facility, so that the relative location of the borescope and the light sheet does not change when the pipe inclination angle is varied. The light sheet is located at an axial distance of $D/\tan 40°$ from the borescope lens. The adopted geometry allows viewing the whole illuminated cross-section of the pipe in the borescope image. The measuring module was located close to the exit from pipe (about 8 m from the pipe inlet). This location insures fully developed flow at the measurement location.

Selection of operational conditions was based on the flow pattern maps obtained by Shoham (1982). Experiments were carried out at three values of liquid superficial velocities: 0.01 m/s, 0.1 m/s and 0.5 m/s; for each liquid flow rate five values of gas superficial velocities were used: 0 m/s, 0.1 m/s, 0.5 m/s, 1.0 m/s, 5 m/s, and 10.2 m/s. For each combination of gas and liquid flow rates experiments were carried out for the following values of pipe inclination angles: $-1°$, $-5°$, $-10°$, $-30°$, $-50°$. Results are presented for those sets of flow conditions where either stratified or slug flow pattern with relatively short liquid slugs and very long elongated bubbles (of the order of 1 m in length) were observed.

In an effort to determine the interfacial wave celerity, capacitance wave gauges were installed along the pipe axis downstream of the borescope in a special transparent module. The outputs of wave gauges were sampled simultaneously with the video recording of the borescope images. No calibration of the wave gauges was carried out. Celerities of long waves can be determined by cross-correlating outputs of wave gauges pairs. Visualization of the flow around the wave gauges revealed, however, that cavitation bubbles are often formed at the wave gauge wires, especially at higher liquid velocities, thus rendering quantitative celerity measurements not reliable and mainly restricted to relatively low liquid velocities. More details about the capacitance wave gauges used in the present study and their limitations are given in Trostinetsky et al. (2004) and Trostinetsky (2005).

3. Data processing

For each inclination angle of the pipe and for each gas and liquid flow rate considered, a short video clip that contained an ensemble of about 1500 individual images for the Sony camera and up to 5000 images when the Pixelink camera was used, was recorded. Green fluorescent dye is added to water in order to increase color contrast between liquid and gas. Digital image processing is necessary to extract quantitative information from the recorded video clips. An example of an individual image recorded by the Sony camera is presented in Fig. 3.

Since the processing is performed on each recorded image separately, the video clip has to be converted into a sequence of separate snapshots for further processing. The whole image processing was performed in MATLAB.

As the first step, the image of the illuminated empty pipe is recorded to serve as a reference. This reference image is then subtracted from every processed frame, in order to receive only pipe contents image. The resulting image is further enhanced to increase the contrast between the areas occupied by water and air. The function maps the grey level values (default values are from 0 to 1) from source image to a new image with a smaller, manually defined gray level range.

Water interface is then determined by application of edge detection. After the edge detection process, the liquid phase contour is obtained. Only the upper boundary of the contour is of interest as it represents the

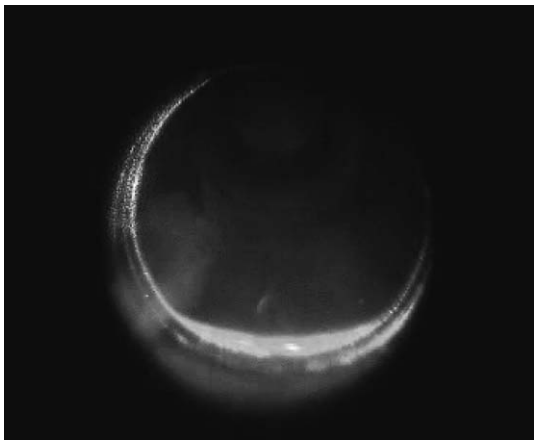

Fig. 3. Typical instantaneous snapshot ($\beta = -10°$, $U_{LS} = 0.1$ m/s, $U_{GS} = 5$ m/s).

liquid–gas interface. The location of the water–air interface in term of real water depth is found using a fitting curve that inverse location in pixels to the real coordinates of the pipe. Such an converts is not one to one because of optical distortions, which arise since the borescope is inserted at 20° relatively to the pipe axis, whereas the imaged plane coincides with the light sheet that is normal to the pipe axis.

For the calibration purpose, a disc with a diameter identical to that of the pipe with a rectangular grid is inserted into the pipe normally to the pipe axis at the light sheet location (Fig. 4).

Only vertical image distortion is significant. Calibration using the disk yields a fitting curve that was obtained based on the observed distances in pixels between the grid lines in the calibration image and their vertical coordinates in mm. The actual coordinates of the gas–liquid interface were calculated accordingly to the fitting curve that was derived from the calibration disc image. The mean physical pixel size in the images is equivalent to about 0.13 for the Sony camera and about 0.03 mm for the higher resolution Pixelink video camera. Due to vertical distortion the pixel size varies somewhat depending on its spatial location.

The preliminary experiments demonstrated that while in the central region of the pipe accurate information on the instantaneous surface elevation is obtained, this is not the case close to the pipe wall. Due to the limited resolution of the recorded images and reflections from the pipe walls, it is always difficult to obtain reliable information in the wall region. On the other hand, the ''climbing'' of the liquid film on the walls and the gradual transition from stratified to annular flow with increasing inclination angle is of particular interest in downward flow. In many cases, the liquid film near the walls is very thin (of the order of few pixels) which makes it

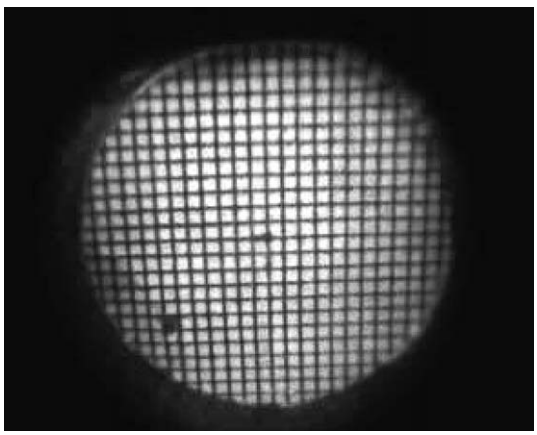

Fig. 4. An image of the calibration disc with the rectangular grid.

very difficult to derive the real height of the climbing film from the recorded image. To overcome the problem of accurate measurements near the pipe wall, a very simple yet effective method was applied. Measuring tape was attached to the pipe periphery from the outside and the circumferential coordinate of the mean border of film climbing was visually determined. When the horizontal and the vertical coordinates of every point of the interface are known, the array containing this information is recorded. Then the averaged values of the interfacial shape are computed. In this procedure, the closest points to the wall that are reliably detected from the image processing are connected to the end points near the pipe wall, which were estimated using the measuring tape.

The process of averaging the data recorded in each individual snapshot for the given flow conditions is complicated by three possible factors. First, the interface curve obtained as a result of the edge detection procedure may not be continuous, in other words, gaps are possible. The interface length can differ from picture to picture, so that the arrays representing each curve may differ in size. In addition, as mentioned above, in many images the thin liquid layer climbing to the pipe wall is hardly detectable. The ways to deal with those problems are now presented.

The "gaps" in the recorded interface are filled by linear interpolation. For every horizontal location, averaged vertical interface coordinate is computed. Only those realizations that have recorded interface at a given horizontal location are taken into account in the averaging procedure.

The problem of the edges of the average interface was solved using results obtained with the measuring tape as described above. The edge point known from the tape and the mean interface shape determined from the borescope measurements are connected by a curve using the spline algorithm. Cubic interpolation is used to get smooth fitting.

In the present experiments, the illumination source is on the left side of the image. In several cases the light sheet does not illuminate uniformly the whole pipe cross-section, due to light sheet dispersion by the complex instantaneous shape of the interface. As a result of it, the right side of the obtained images is not always sufficiently sharp. In these cases it is reasonable to take the interface as a symmetric one, with the right half as a mirror reflection of the left side.

Errors in the borescope-derived data result from a number of factors. First, the interface contrast in the images is not always sharp as in Fig. 3. Under certain conditions, in particular when the gas–liquid interface is highly disturbed, blurred images may appear, leading to errors in processing. An example of such an image is given in Fig. 5. The water depth in the recorded images is determined by the edge detection procedure as described above. The edge detection algorithm is sensitive to the image intensity gradient. The threshold applied in the edge detection is determined by visual inspection. Fig. 6 shows the output of the edge detection procedure applied to the image of Fig. 5 with two different threshold values and illustrates the effect of the threshold selection on the edge location when applied to the raw image of Fig. 6.

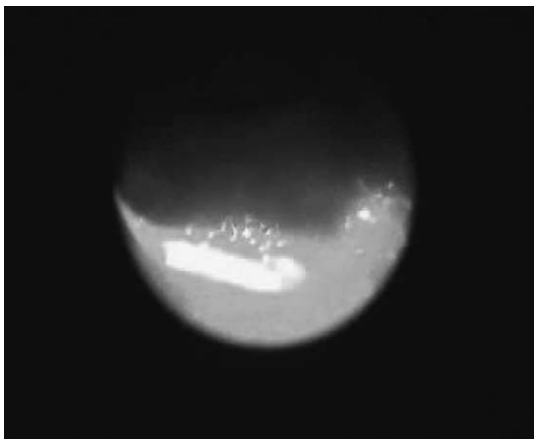

Fig. 5. Example of a blurred borescope image.

Fig. 6. Water–air interface contours after edge detection for two different threshold values.

It is clear from this figure that for both threshold values selected, the lack of sharp border may cause ambiguity in the interface location. This ambiguity is usually less prominent in the left part of the image since, as stressed above, the light sheet at the right part of the image may become somewhat diffused by the irregularities of the interface. In case when multiple interface locations are obtained as a result of the applied detection algorithm, the uppermost output is selected for every horizontal location. The upper horizontal line in Fig. 6 denotes the vertical location of the maximum surface elevation at the left part of the pipe, whereas the lower line marks the minimum surface elevation. Both lines are drawn based on the left image of Fig. 6. By comparing the locations of the appropriate points in the right-hand image of the same figure, it becomes obvious that the ambiguity in the threshold can be estimated to be about 3–5 pixels. The physical pixel size in the images is equivalent to ~0.10–0.15 mm (depending on the camera focus length used in the particular recording session).

Additional source of the errors is related to the translation from pixels to millimeters using the calibration procedure based on the calibration disk. This error is estimated not to exceed several pixels. The cumulative maximum overall error for average water depth values resulting from all those reasons is estimated as about 6 pixels, corresponding to 0.7–1.0 mm.

The geometrical parameters that can be directly extracted using the visualization technique, are: cross-sectional instantaneous interface shape, instantaneous void fraction, interfacial wave characteristics, including the values of depth fluctuations at various locations in the pipe cross-section. The actual velocities of water and gas phases can then be calculated from the measured void fraction and the corresponding superficial velocities. These geometrical parameters can also be employed to estimate the relative contribution of various terms in the momentum balance equation.

The interface shape averaged over the whole ensemble of instantaneous images for any given set of flow parameters is computed. To this end, the coordinates of the interface detected in each frame are averaged over the whole ensemble for each horizontal location, x, separately. An example of the ensemble-averaged interfacial shape is given in Fig. 7. The central line represents the mean interface shape $\bar{h} = \bar{h}(x)$. The RMS values of the fluctuations in y are also determined in the course of the image processing. Upper and lower lines in Fig. 7 correspond to the average shape plus and minus the RMS values.

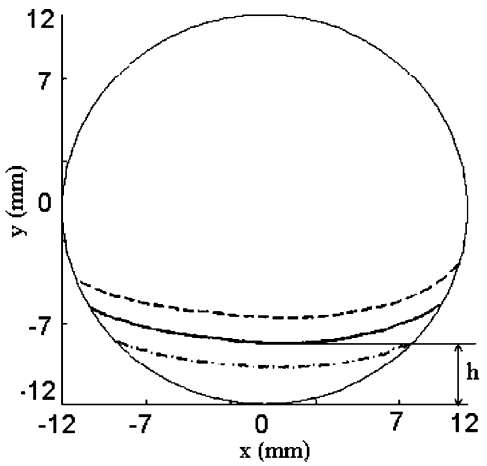

Fig. 7. Ensemble-averaged interfacial shape and its fluctuations ($\beta = -70°$, $U_{LS} = 0.023$ m/s, $U_{GS} = 10$ m/s). The central line represents the mean water depth, while the upper and the lower lines represent the mean ± RMS values, respectively.

4. Results

Water depth at the vertical pipe symmetry axis is averaged over all images recorded at any given flow conditions. Average variation of $\bar{h}(x=0)$ is presented in Fig. 8 as a function of the gas superficial velocity U_{GS} and pipe inclination β. Even small angles of inclination relative to horizontal cause a dramatic decrease in the water depth. For horizontal flow, water depth $\bar{h}(x=0)$ decreases as the gas velocity increases.

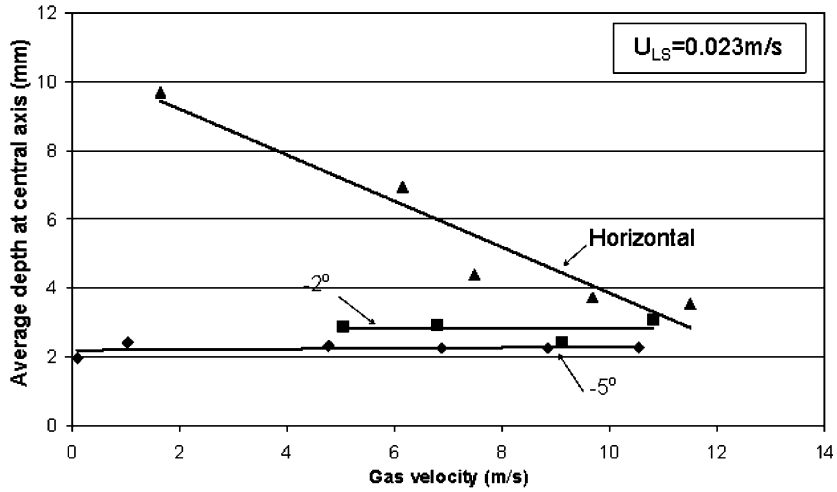

Fig. 8. Average depth variation as a function of gas velocity for small inclination angles. The cumulative maximum error in depth is estimated to be 0.7–1.0 mm.

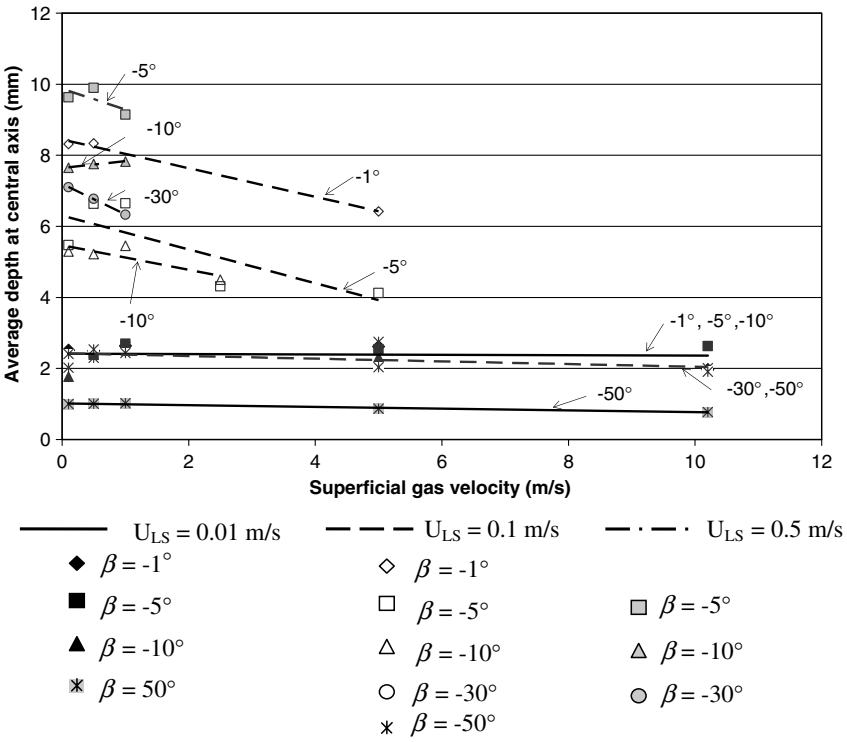

Fig. 9. Average depth variation as a function of gas velocity for small inclination angles. The cumulative maximum error is as in Fig. 8.

Averaged water depth $\bar{h}(x = 0)$ is shown in Fig. 9 as a function of the gas superficial velocity U_{GS}, for different liquid superficial velocities U_{LS} and pipe inclinations. For the low liquid flow rate ($U_{LS} = 0.01$ m/s), the measured average depth is about 2 mm and remains insensitive to the gas flow rate variation as well as to pipe inclinations in the range from $-1°$ to $-10°$ and for that reason is represented by a single trend line in this figure. At steeper inclination of $-50°$, the mean water depth decreases significantly to about 1 mm. At higher liquid flow rates of $U_{LS} = 0.1$ m/s and $U_{LS} = 0.5$ m/s, the mean water depth increases notably and is strongly dependant on the pipe inclination angle. The mean water depth decreases as the pipe inclination becomes steeper, yet remains similar for relatively high inclinations of $-30°$ and $-50°$. The effect of the gas velocity is relatively weak, becoming somewhat more pronounced for higher values of U_{LS} and the corresponding increase in the water layer depth.

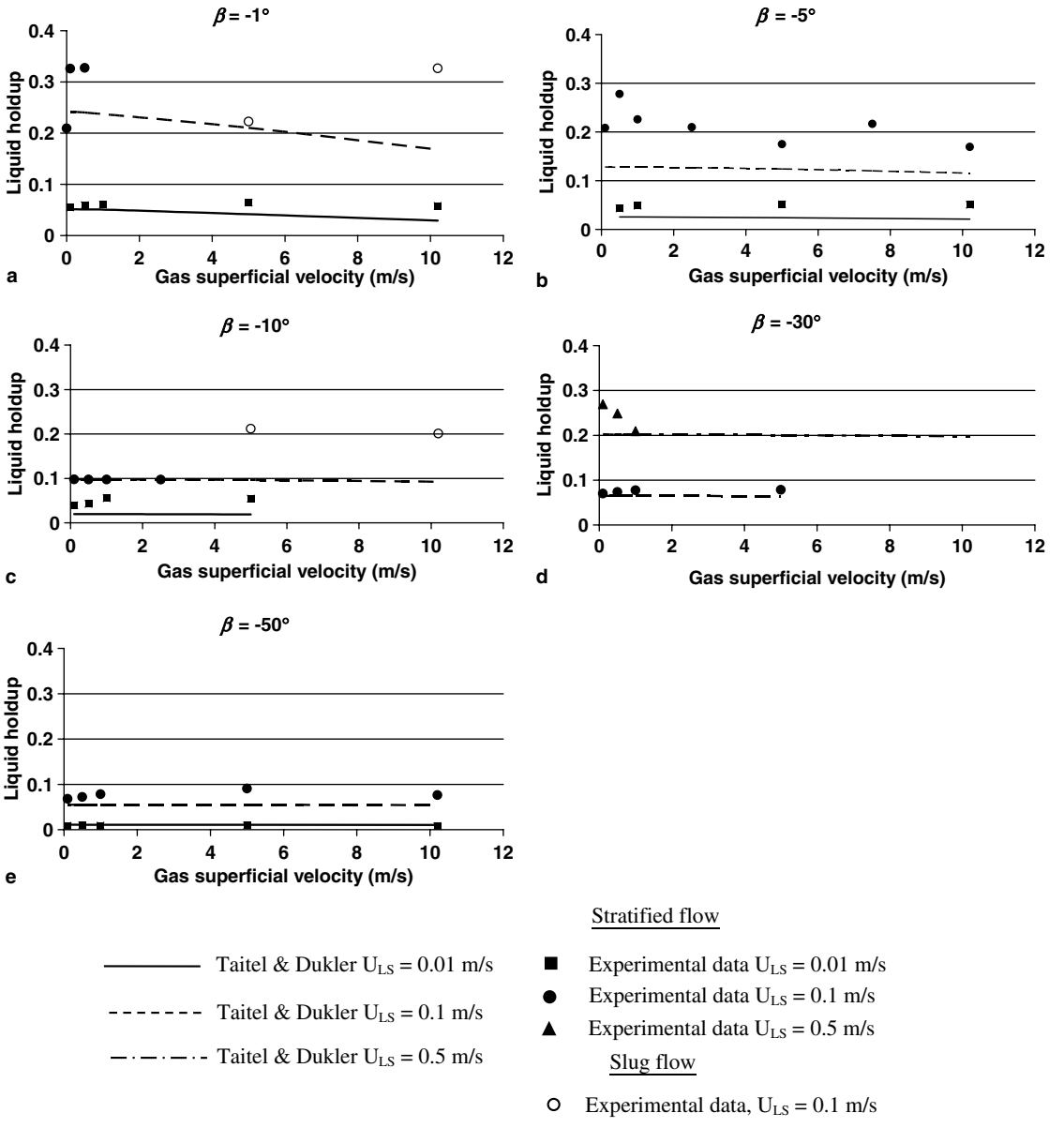

Fig. 10. Liquid holdup comparison between experimental data and Taitel–Dukler model. The error in determination of superficial velocity and in liquid holdup is estimated not to exceed 10%.

Experimental data on the liquid holdup are compared in Fig. 10 with the predictions of Taitel and Dukler (1976) model for stratified flow. Two assumptions are made in the model calculations: that the interface is flat and that the interfacial friction coefficient is equal to that of the gas on the pipe wall. Results of Fig. 10 indicate that the discrepancy usually does not exceed about 20%. This agreement can be considered as reasonable considering crude approximations made in the model calculations. Similar agreement between the present experiments and Taitel–Dukler model estimates is obtained when water depth levels are compared.

In view of the weak dependence of the mean depth $\bar{h}$ on U_{GS}, it makes sense to consider averaging of $\bar{h}(x=0)$ over all gas velocities U_{GS} employed for given U_{LS} and pipe inclination β. The effect of the pipe inclination angle on $\bar{h}(x=0)$ averaged over different U_{GS} is shown in Fig. 11 for all liquid flow rates employed.

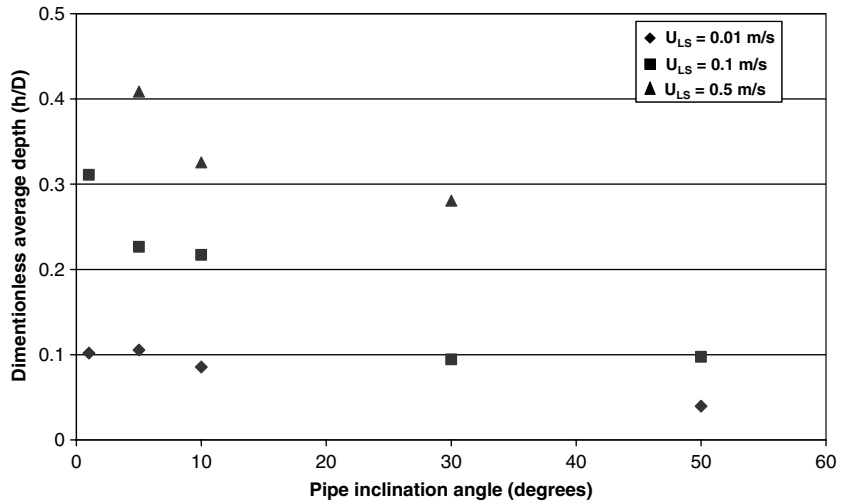

Fig. 11. Dimensionless average depth $\bar{h}(x=0)/D$ as a function of the pipe inclination angle β.

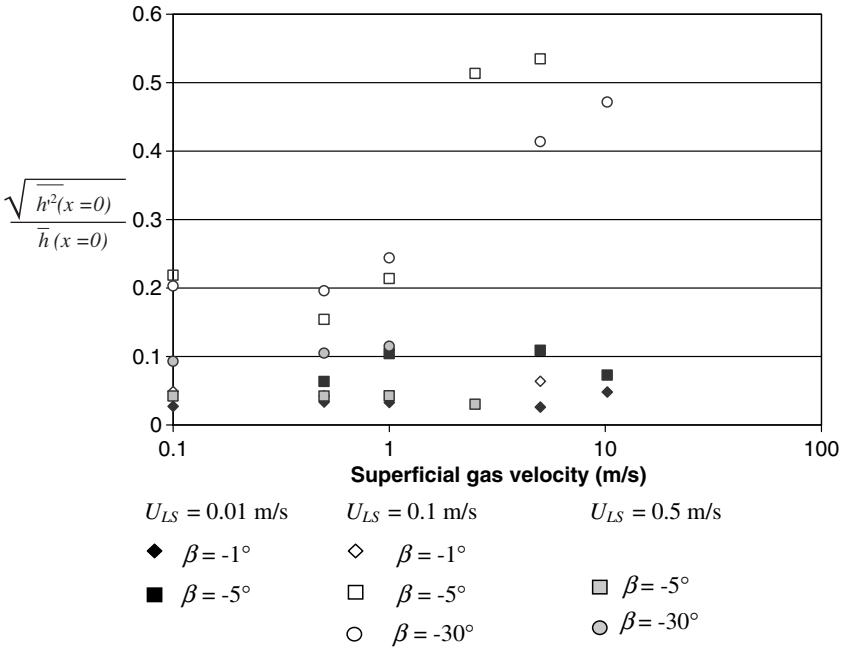

Fig. 12. Normalized RMS values of water depth fluctuations on the vertical central line of the pipe cross-section.

The figure clearly demonstrates that the average water depth decreases with increasing pipe inclination. This can be attributed not only to the obvious effect of the increase in the liquid velocity for steeper downward pipe inclinations due to gravity, but also to the fact that for higher absolute values of β, the liquid–gas interface becomes more concave, with liquid layer climbing at the pipe wall, as will be shown in sequel.

The instantaneous liquid layer depth at any specific location in the pipe cross-section $h(x,t)$ can be derived from the video-recorded sequence of the borescope images. The instantaneous water depth at any horizontal location x can be presented as $h(x,t) = \bar{h}(x) + h'(x,t)$. The variation in time of water depth h at $x = 0$ of the pipe cross-section is considered first. The magnitude of fluctuations of the water layer depth $h'(x,t)$ can be characterized by their root mean square (RMS) values $\sqrt{\overline{h'^2}}$. The values of $\sqrt{\overline{h'^2}}(x=0)$, normalized by the mean depth $\bar{h}(x=0)$, are presented as a function of gas superficial velocity U_{GS} for representative inclination angles and liquid flow rates U_{LS} in Fig. 12. At low liquid flow rate, the relative fluctuation values remain low for all gas flow rates and usually do not exceed about 10%. At higher flow rate, $U_{LS} = 0.1$ m/s, the fluctuations relative to the mean water level become larger and seem to increase with gas flow rate. At even higher flow rate of $U_{LS} = 0.5$ m/s, the mean water level $\bar{h}(x=0)$ becomes relatively deep, resulting in a slight decrease of the relative RMS fluctuation values. The results in Fig. 12 show only those cases where stratified flow regime was observed and do not contain conditions at which slug flow regime was observed at higher gas flow rates.

The variation of the instantaneous surface depth h with time allows identifying a number of distinct interfacial patterns. The simplest case is the smooth stratified flow regime where the fluctuations in h mostly do not exceed a single pixel.

At steeper inclinations and higher flow rates the gas–liquid interface becomes wavy. Spectral analysis of the recorded time series $h(x,t)$ enables to determine characteristic frequencies of surface waves.

The unique ability of the borescope to provide instantaneous water depth at different locations across the pipe as a function of time enables not only to determine the frequency contents of the interface waves, but also to express quantitatively the two-dimensionality of the interfacial waves by using the cross-correlation coefficient of the instantaneous depth fluctuations defined as

$$r(x/R) = \frac{\overline{h'(0)h'(x/R)}}{\sqrt{\overline{h'(0)^2}}\sqrt{\overline{h'(x/R)^2}}} \tag{1}$$

The overbar in Eq. (1) represents averaging over the whole duration of sampling. The value of $r(x/R)$ close to unity for all x indicates a plane wave, whereas fast decaying with x values of the cross-correlation coefficient correspond to a case when the wave structure is essentially three-dimensional. The cross-correlation coefficient distributions for several flow conditions are presented in Figs. 13–16.

The recorded wave frequency spectra suggest that three wavy stratified flow regimes can be identified: (i) flow dominated by long waves with frequencies below 0.5 Hz; (ii) shorter surface waves with a wider spectrum dominated by higher-frequency (2–5 Hz) waves; and (iii) waves characterized by a double-peaked spectrum.

In Fig. 13 results corresponding to low-frequency waves are presented for shallow pipe inclination of $-5°$ and flow rates given by $U_{LS} = 0.1$ m/s, $U_{GS} = 5$ m/s. The recorded time series of the water level at $x = 0$ is presented in Fig. 13(a), the wave pattern is characterized by mainly low frequency fluctuations around the mean level of about 4.5 mm that can exceed few millimeters. The corresponding amplitude spectrum presented in Fig. 13(b) exhibits a dominant peak at frequency of about 0.3 Hz. The dependence of the corresponding cross-correlation coefficient on the spanwise coordinate is presented in Fig. 13(c). Cross-correlation coefficient remains high (above 0.95) over the whole interface, indicating that the interface structure is basically two-dimensional.

Wave pattern corresponding to the second regime as characterized by the frequency spectra is presented in Fig. 14. Here, at steeper pipe inclination $\beta = -30°$, $U_{LS} = 0.5$ m/s, $U_{GS} = 5$ m/s the mean water depth is somewhat higher than in the previous figure due to higher liquid flow rate. Liquid level fluctuations in this case are shown in Fig. 14(a) and exhibit a notably higher frequency. For that reason, the fluctuations are presented for a relatively short duration of 10 s. The corresponding amplitude spectrum in Fig. 14(b) is wider than in the previous case with dominant frequencies about few Hz. The spanwise correlation coefficient shown in Fig. 14(c), although somewhat lower than in Fig. 13, remains relatively high, indicating that for this wave regime the interface structure maintains strong two-dimensionality.

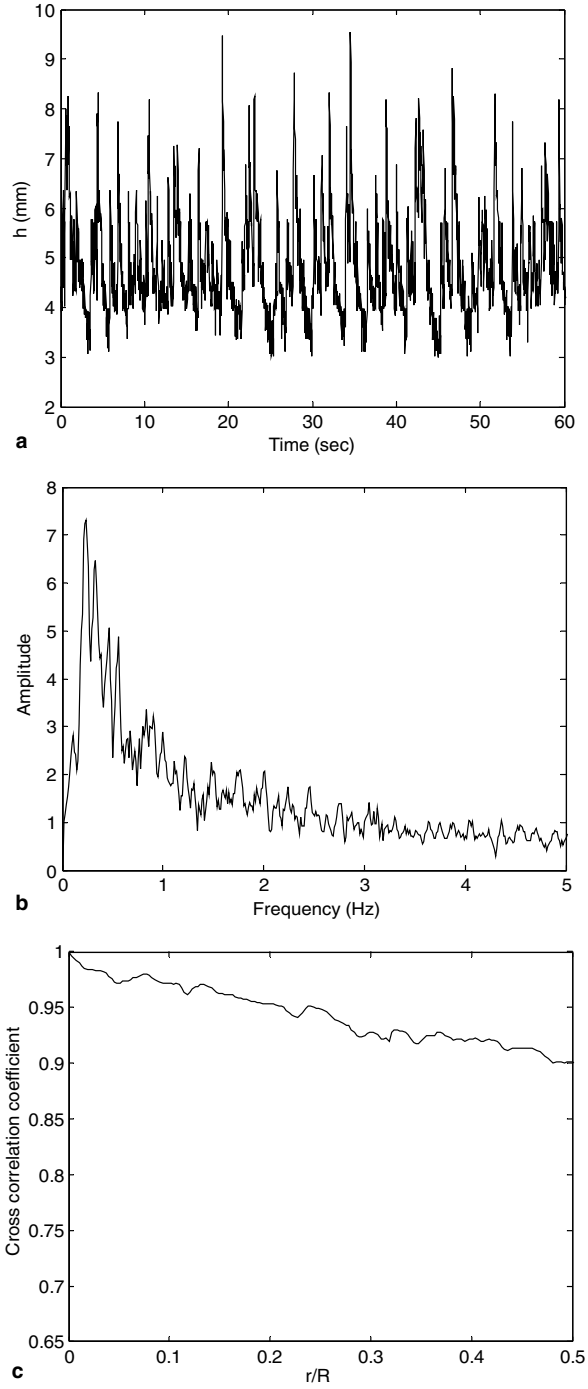

Fig. 13. Interfacial wave structure for $\beta = -5°$, $U_{LS} = 0.1$ m/s, $U_{GS} = 5$ m/s: (a) $h(x = 0, t)$ (in mm) as a function of time; (b) amplitude spectrum of $h(x = 0, t)$; (c) cross-correlation coefficient $r(x)$.

When the liquid flow rate is decreased to $U_{LS} = 0.1$ m/s while all other parameters are retained as in Fig. 14, the wave pattern somewhat changes, Fig. 15. The mean water level is now slightly above 3 mm, whereas high-amplitude level fluctuations occur more often, Fig. 15(a). The spectrum of water level fluctuations, Fig. 15(b), reveals two dominant peaks, the first corresponding to low frequency oscillations, resem-

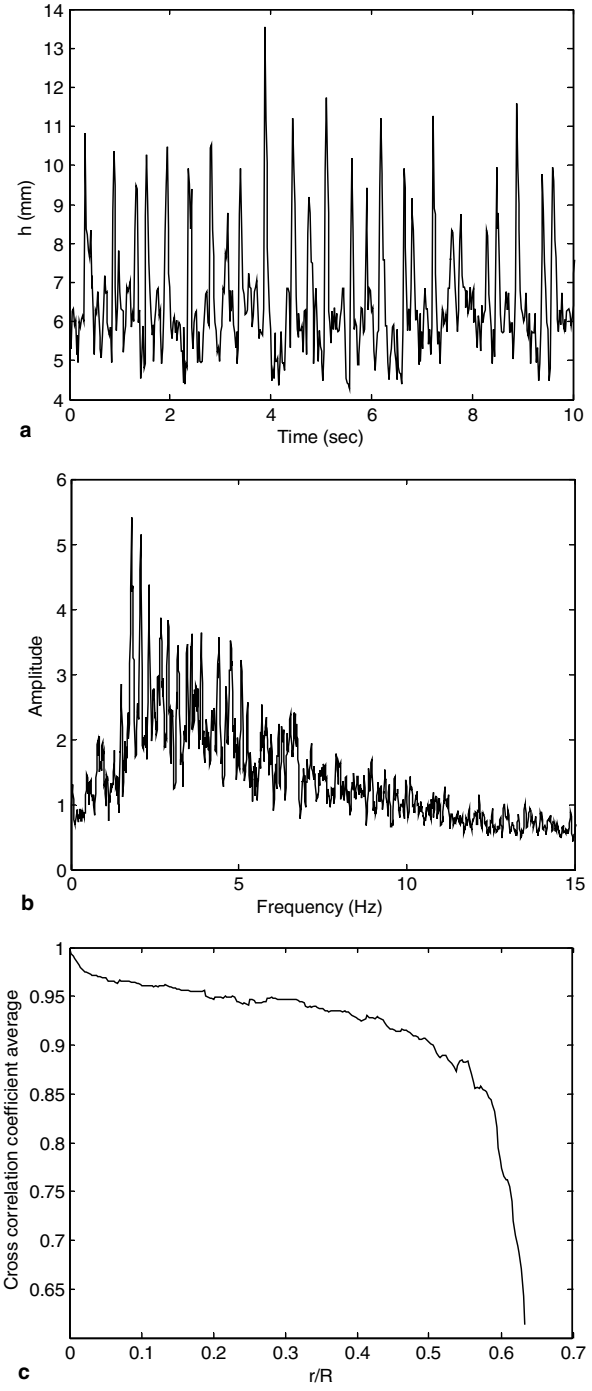

Fig. 14. As in Fig. 10 for $\beta = -30°$, $U_{LS} = 0.5$ m/s, $U_{GS} = 5$ m/s.

bling the peak in Fig. 13(b), and the wider peak at higher frequencies, similar to that in Fig. 14(b). The cross-correlation coefficient for these flow conditions remains above the value of 0.9 for the whole extent of the interface.

At steep pipe inclinations in Figs. 14 and 15, the level fluctuations are dominated by high-amplitude waves with maximum amplitudes of the order of the mean water level. These waves are predominantly

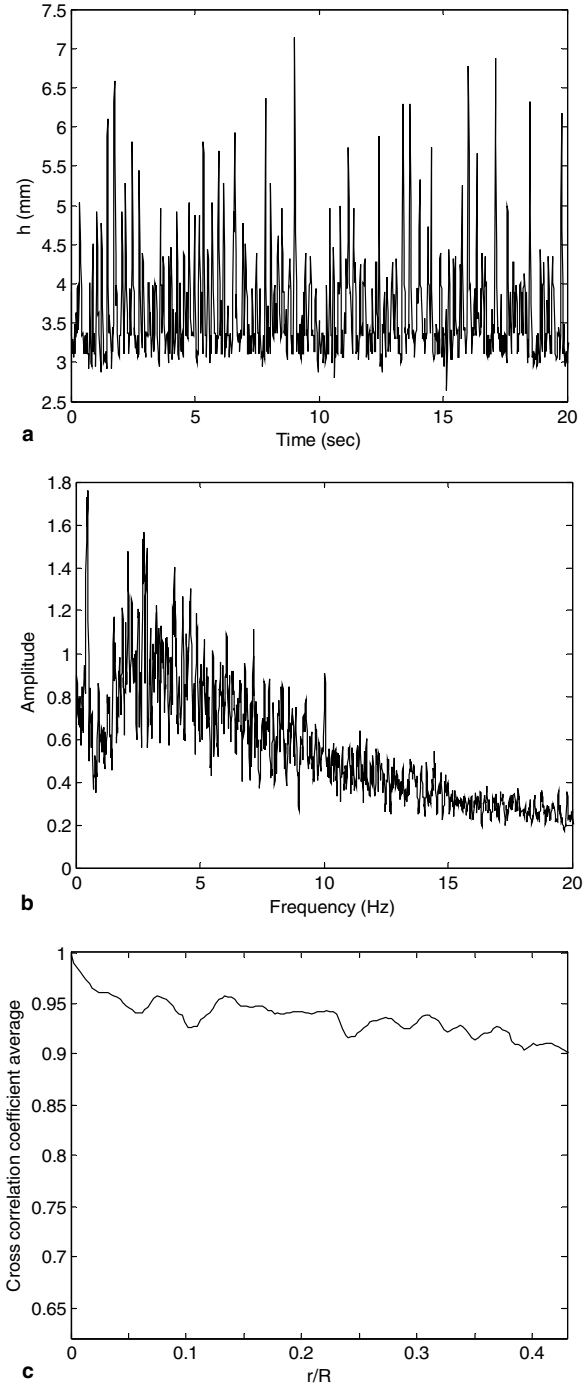

Fig. 15. As in Fig. 10 for $\beta = -30°$, $U_{LS} = 0.1$ m/s, $U_{GS} = 5$ m/s.

two-dimensional. At lower inclination angles, the maximum amplitudes are notably smaller and usually do not exceed 1 mm. The typical temporal variation of the instantaneous water level for $\beta = -10°$, $U_{LS} = 0.5$ m/s, $U_{GS} = 0.1$ m/s is presented in Fig. 16(a). The amplitude spectrum in this case, Fig. 16(b), is wide and resembles that in Fig. 14(b), but the spanwise structure of the waves is essentially three-dimensional, as demonstrated by fast decay of the cross-correlation coefficient, Fig. 16(c).

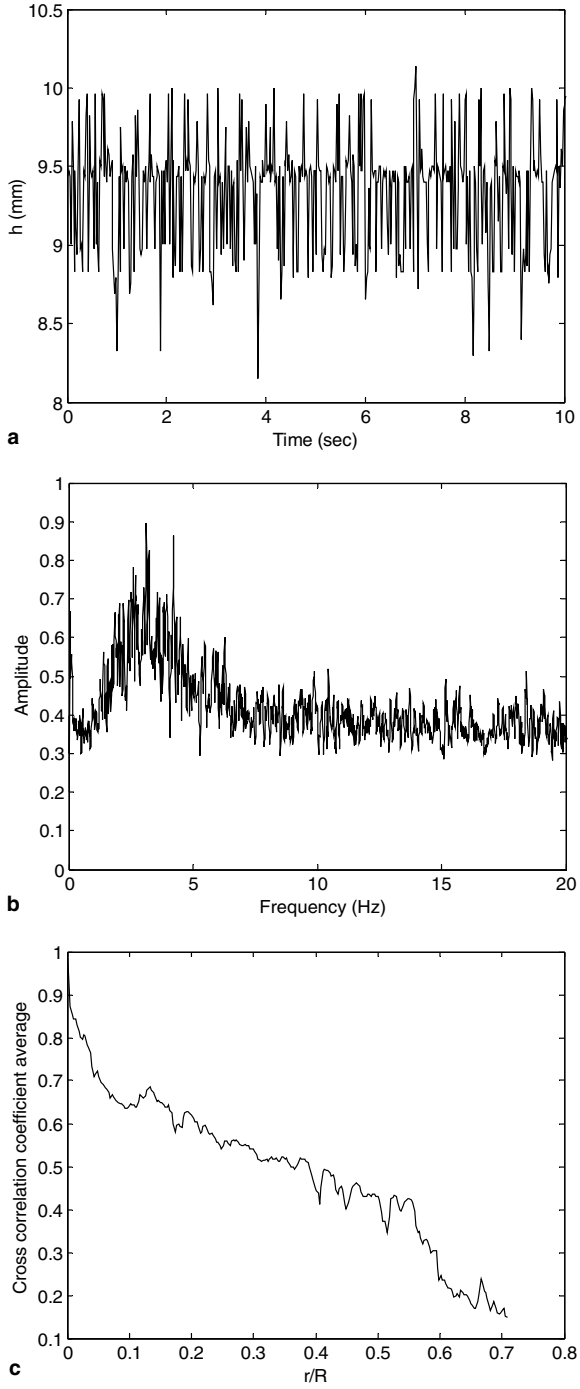

Fig. 16. As in Fig. 10 for $\beta = -10°$, $U_{LS} = 0.5$ m/s, $U_{GS} = 0.1$ m/s.

It seems that transition between the liquid–gas interface structure patterns in stratified downward flow can be specified as a function of the actual liquid velocity and the liquid depth. Smooth interface with long waves of vanishing amplitude is observed for low liquid velocities and shallow liquid level only. For deeper water level and liquid velocities not exceeding 0.5 m/s, or somewhat higher liquid velocities and very shallow water level around 1 mm, gradual increase in the amplitude of the low frequency waves occurs. In deeper

water above 2 mm, the interface is dominated by higher frequency waves with wide spectrum. Binary frequency system is observed in a narrow domain of liquid velocities of about 1–1.5 m/s and water depth around 2 mm.

While mainly of qualitative nature and limited in scope, the wave celerity measurements performed in the present study using capacitance wave gauges, enable relating the measured dominant frequencies with the corresponding wave lengths at the gas–liquid interface. At low liquid velocities, the wave gauges measurements indicate that the wave celerity is only somewhat higher than the actual liquid velocity. At higher liquid velocities, where the application of capacitance wave gauges was not possible as described in Section 2, it can be assumed that the relative difference between the celerity of shallow water waves and the liquid velocity is even smaller. Using the liquid velocity as the wave propagation velocity allows one to estimate the dominant wave length. This length appears to be in the range from about 0.4 m to about 1.5 m. The estimated length of these shallow water waves agrees qualitatively with visual observations of the interface structure made in the course of the experiments. The shorter ripples could not be quantitatively measured using wave gauges because of appearance of air bubbles at the gauge wires, whereas the maximum video recording speed of 50 Hz was insufficient to estimate the spectral contents of those ripples.

It is well known that the interfacial shape in gas–liquid stratified flow is not necessarily flat and can vary from convex to concave. Interface configuration depends on various flow parameters, such as pipe diameter, inclination angle, surface tension coefficient, physical properties of the fluids, the gas and liquid holdup and wettability of the solid wall of the pipe, etc.

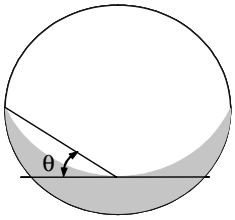

Fig. 17. Definition of the climbing angle θ.

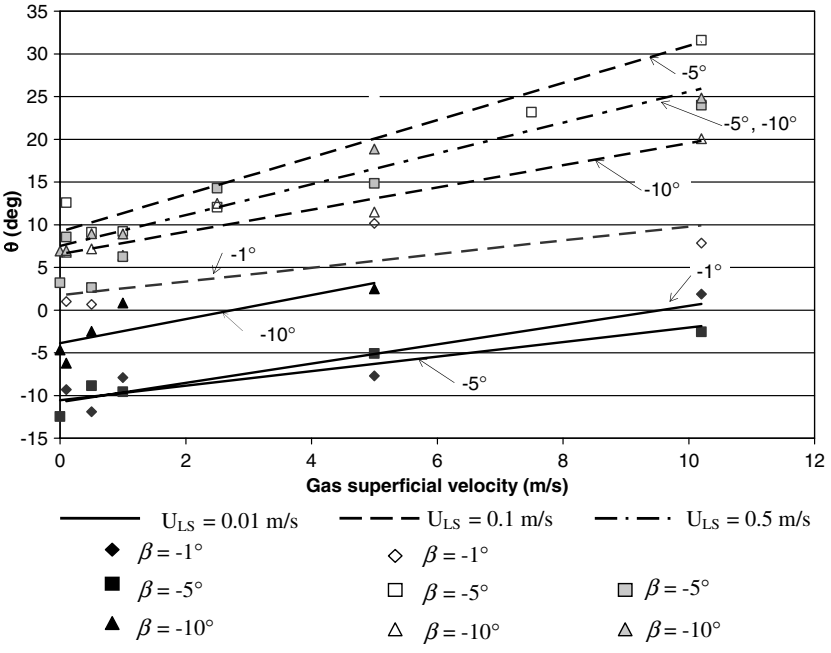

Fig. 18. Climbing angle θ as a function of gas superficial velocity for various pipe inclination angles and liquid superficial velocities.

The present study is carried out in a single pipe with fluids (air and water) of given physical properties, so that interfacial shape is determined by flow rates of both fluids and the pipe inclination angle.

When the interface is not plane, climbing (or declining) of the liquid film along the cross-sectional perimeter can be characterized by the value of the angle θ defined in Fig. 17. The measured values of the climbing angle θ are presented in Fig. 18 for $U_{LS} = 0.01$ m/s and $U_{LS} = 0.1$ m/s. It is clearly seen from this figure that in general, θ increases with increase of $|\beta|$.

For very shallow water layer observed for low liquid flow rates ($U_{LS} = 0.01$ m/s), capillary forces become dominant, causing the convex interface shape and thus negative values of the angle θ. The water depth is very similar for inclinations of $-1°$ and $-5°$; and the corresponding values of θ are very similar. The interface becomes nearly flat for high gas velocities. For $-50°$, the water level is very shallow, thus the film climbing is impossible and the liquid shape remains convex.

For $U_{LS} = 0.1$ m/s and correspondingly deeper water level, the interface becomes more concave. The climbing angle increases with increase in pipe inclination angle and with the gas superficial velocity.

The measured values of the climbing angle θ were compared with the correlation for interfacial curvature suggested by Brauner and Ullmann (2004). Reasonable agreement was obtained.

5. Discussion and conclusions

The feasibility of using a borescope for quantitative measurements in gas–liquid flow studies in pipes is studied in detail. The results of the study demonstrate that a borescope can be effectively used for visualizing two-phase flow within a pipe mainly when a single phase with a constant refraction index exists between the borescope lens and the gas–liquid interface in the illuminated plain.

In the present study the cross-sectional interface shape between gas and liquid in stratified downward pipe flow is investigated. Combination of the results obtained with a measuring tape at the outer surface of the pipe and those derived from the borescope images within the pipe provides a reliable average interfacial shape in the whole cross-section of the pipe. This information enabled us to study the dramatic changes of the gas–liquid interfacial shape that occurs in downward inclined pipe flow as a result of variation of the pipe inclination and the gas flow rate. The gradual transition from a relatively plain interface in the stratified flow regime to high climbing angles in the course of transition to annular flow is documented. This gradual climbing of the liquid film around the pipe circumference may result from different mechanisms. At low gas flow rates, the increasing climbing angle is a direct outcome of reduced effective gravity at steeper pipe inclination, whereas at higher gas velocity the effect of the shear stress at gas–liquid interface becomes important.

An additional essential advantage of the present technique is in its ability to determine the two-dimensional structure of the complex time-dependent interface that is characterized by waves of various scales. The computations of the spatial cross-correlation coefficients allow providing quantitative estimates of the interfacial waves structure. The dominant frequencies in the sequence of the borescope-derived interface level fluctuations increase with actual liquid velocity. It appears that the length of the most energetic waves is of the order of 1 m, in agreement with visual observations. In a relatively narrow domain of liquid velocities and pipe inclinations bi-modal frequency spectrum was obtained, indicating that at those conditions even longer waves are also essential. The long waves are characterized by high spatial coherence and the interface therefore can be considered as dominantly one-dimensional. However, when shorter ripples (with the length of the order of few centimeters, as observed in the course of the experiments) become strong, the spatial cross-correlation coefficient decays fast and the interface is essentially two-dimensional.

Due to the technical limitations of the present flow visualization set-up, no video recording was possible at frequencies higher than 50 Hz. To substantiate the borescope-derived results, an attempt was made to use a number of wave gauges, placed along the pipe axis, to record fast variations in the water level depth. In addition, cross-correlation of the wave gauges outputs enables to make estimates of long wave celerities and thus to evaluate the characteristic wave lengths from the frequency spectra. However, the present experiments show that the wave gauges can hardly be applied effectively due to large air bubbles attached to the gauges at relatively high liquid velocities that prevent quantitative measurements.

With all its limitations, borescope-based measurements appear as a powerful and inexpensive method that allows recording of the instantaneous gas–liquid interfacial shape in the whole pipe cross-section. Both the

spatial resolution and the data acquisition rate of the borescope-derived images are determined by the recording video camera. Even with a simple digital video camera used in most experimental runs of this study, the spatial resolution attained was substantially better than that achieved by alternative means, such as various realizations of tomography.

Acknowledgements

The authors gratefully acknowledge support for this study by the grant # 200/03 from the Israeli Science Foundation.

References

Angeli, P., Hewitt, G.F., 2000. Drop size distributions in horizontal oil–water dispersed flows. Chem. Eng. Sci. 55, 3133–3143.

Barnea, D., Shoham, O., Taitel, Y., 1982. Flow transition for downward inclined two phase flow; horizontal to vertical. Chem. Eng. Sci. 37, 735–740.

Brauner, N., Ullmann, A., 2004. Closure relation for two-fluid models for stratified flow in the smooth and wavy regimes. In: 42nd European Two-Phase Flow Meeting, Genoa, Italy.

Giovine, P., Minervini, A., Andreussi, P., 1991. Stability of liquid flow down an inclined tube. Int. J. Multiphase Flow 17, 485–496.

Luninski, Y., Barnea, D., Taitel, Y., 1983. Film thickness in horizontal annular flow. Can. J. Chem. Eng. 61, 621–626.

Paras, S.V., Vlachos, N.A., Karabelas, A.J., 1994. Liquid layer characteristics in stratified-atomization flow. Int. J. Multiphase Flow 20, 939–956.

Shoham, O., 1982. Flow pattern transition and characterization in gas–liquid two phase flow in inclined pipes. Ph.D. Thesis, Tel-Aviv University.

Taitel, Y., Dukler, A.E., 1976. A theoretical approach to the Lockhart Martinelli correlation for stratified flow. Int. J. Multiphase Flow 2, 591–595.

Trostinetsky, E., 2005. Application of borescope to studies of gas–liquid flow in downward inclined pipes. M.Sc. Thesis, Tel-Aviv University.

Trostinetsky, E., Shemer, L., Barnea, D., 2004. Interfacial shape and interfacial shear stress in downward stratified gas–liquid pipe flow. In: 42nd European Two-Phase Flow Meeting, Genoa, Italy.

Wojtan, L., Ursenbacher, T., Thome, J.R., 2003. Measurement of dynamic void fractions in stratified types of flow. In: 3rd European-Japanese Two-Phase Flow Group Meeting, Siena, Italy, pp. 21–27.